Active screen plasma surface co-alloying treatments of 316 stainless steel with nitrogen and silver for fuel cell bipolar plates

Lin, Kaijie; Li, Xiaoying; Tian, Linhai; Dong, Hanshan

DOI:
10.1016/j.surfcoat.2015.10.038

Document Version
Peer reviewed version

Citation for published version (Harvard):
Lin, K, Li, X, Tian, L & Dong, H 2015, 'Active screen plasma surface co-alloying treatments of 316 stainless steel with nitrogen and silver for fuel cell bipolar plates', *Surface and Coatings Technology*, vol. 283, pp. 122-128. https://doi.org/10.1016/j.surfcoat.2015.10.038

Active screen plasma surface co-alloying treatments of 316 stainless steel with nitrogen and silver for fuel cell bipolar plates

Kaijie Lin, Xiaoying Li, Linhai Tian, Hanshan Dong

PII: S0257-8972(15)30335-2
DOI: doi: 10.1016/j.surfcoat.2015.10.038
Reference: SCT 20652

To appear in: *Surface & Coatings Technology*

Received date: 16 June 2015
Revised date: 16 September 2015
Accepted date: 19 October 2015

Please cite this article as: Kaijie Lin, Xiaoying Li, Linhai Tian, Hanshan Dong, Active screen plasma surface co-alloying treatments of 316 stainless steel with nitrogen and silver for fuel cell bipolar plates, *Surface & Coatings Technology* (2015), doi: 10.1016/j.surfcoat.2015.10.038

Active screen plasma surface co-alloying treatments of 316 stainless steel with nitrogen and silver for fuel cell bipolar plates

Kaijie Lin*, Xiaoying Li, Linhai Tian, Hanshan Dong

School of Metallurgy and Materials, The University of Birmingham, Birmingham B15 2TT, UK

Abstract

Due to their good mechanical and corrosion properties, relatively low cost and ease of manufacture, 316 austenitic stainless steel has been researched as a promising candidate material for bipolar plates in proton exchange membrane fuel cells. However, its interfacial contact resistance (ICR) is about 16 times higher than that of the Department of Energy target(10 $m\Omega\ cm^2$), which leads to undesirable fuel cell performance. In this work, active screen plasma (ASP)surface co-alloying treatments with both nitrogen and silver were developed to modify the surface of 316 stainless steel to reduce its ICR required for high-performance bipolar plates. The treated surfaces were fully studied by means of scanning electron microscopy, X-ray diffraction, glow discharge optical emission spectroscopy and energy dispersive spectroscopy. The experimental results demonstrated that a duplex surface layer structure consisting of an Ag-rich surface deposition layer supported by an S-phase case was generated by the ASP surface co-alloying treatment. TheASP co-alloying treated surfaces showedincreased corrosion potential andreduced corrosion current density, and significantly improved surface electrical conductivity. This could be attributed to the introduction of metallic Ag particles by this novel surface plasma treatment.

Keywords: active screen plasma, 316 stainless steel, co-alloying, nitrogen, silver, bipolar plate

*Corresponding author: email linkaijie12@gmail.com; phone +44 (0) 121 414 5197

1 Introduction

Because of the ever-increasing concerns over the depletion of fossil fuel and the aggravation of greenhouse gas emission, considerable research has recently been conductedto develop alternative methods of power generation. Among them, the proton exchange membrane fuel cell (PEMFC) has been considered as one of the most promising candidate in stationary and transportation applications due to itshigh efficiency, near zero emission, low working temperature and fast start-stop behaviour[1].

Bipolar plates are the key multi-functional components in PEMFCs and graphite has been currently employed to makethe bipolar platesdueto its good corrosion resistance and electrical conductivity in PEMFC working conditions. However, the inherent poor mechanical propertiesand the unacceptably high manufacturing cost are barriersto their widespread use.

Comparedwith graphite, stainless steels (SS) exhibit a much higher mechanical strength and a much lowermanufacturing cost, and have attracted massiveinterest for bipolar plate applications[2][3][4]. It is known that stainless steels possess satisfactory corrosion resistance for many applications. The inherent passive film formed on the stainless steel surface, however,greatly increases the interfacial conduct resistance (ICR), leading to the degradation of output power of fuel cells.Therefore, surface modification is needed to improve thesurface conductivityof stainless steels[5].

Silver is well known for its excellent electrical conductivity and chemical stability, and it has beenapplied to improve the surface properties of stainless steel bipolar plates via surface modification technologies. Ag coated 316 SS bipolar plates by electrodeposition methods [6] [7] show significantly improved surface electrical conductivity. The unavoidable defects (such as pin-holes) in the coating, however, are found to act as the short-cut for the penetration of corrosive solution to reach the substrate in the acidic environment, resulting in

the failure of Ag coatings. In view of the shortcoming of coating technology, Feng [8]alloysthe 316 SS surfacesby ion implantation method and the Ag implanted 316L SS shows enhanced corrosion resistance and polarization resistance. The ICR value is reduced after the treatment, butit is still much higher than the target set by the Department of Energy (DOE), mainly due to the formation of silver oxide.

Recently, the authors have explored the possibility of improving the surface electrical conductivity of 316 SS by low-temperature active-screen plasma nitriding (ASPN)[9]. The ASPN treatment can significantly reduce the ICR from 158 mΩ cm^2 for the untreated 316 SS to 33 mΩcm^2, which is still higher than the DOE target of 10 mΩ cm^2. In the present work, a new active screen plasma co-alloying technologyhas beendeveloped to introduce both nitrogen and silver into 316 stainless steel surfaces aiming at further improving the surface electrical conductivityof 316 SS.

2 Experimental

Commercial 316austenitic stainless steel wasused in this study as the substrate material and its chemical composition (wt%) is 0.06C, 17.20Cr, 1.30Mn, 2.20Mo, 11.70Ni, 0.014S, 0.026P, 0.60Si, with Fe balanced. Samples of 6mm in thickness and 25.4 mm in diameter werecut from hot rolled bars. The surfaces of the samples to be treated werewet ground from #120 up to #1200 grit using SiC emery paper, followed by polishing using diamond paste from 6μm down to 1μm.Prior to plasma treatment, the polished samples were degreased with acetone in an ultrasonic bath for 10 min and finally dried with flowing hot air.

Cross sections were cut from the treated samples and mounted in conductive backlite, followed by the same preparation procedures as described above. An etching agent containing 25% H_2O+25% HNO_3+50% HCl was used to reveal the micro-structure of the cross sections.

Active screen plasma co-alloying with nitrogen and silver (ASPA(N&Ag))treatmentswerecarried out in a 40 kW Klöckner conventional DC plasma nitriding furnace with a laboratory active screen set-up, the details of which could be found elsewhere [10]. However, in order to achieve co-alloying with not only N but also Ag, the lid of the metal mesh cylinder (i.e. active screen) wasfabricated by hot isostatic pressing (HIP),using the powdermixture of 95% 316L stainless steel and 5% silver. The active screen plasma co-alloying treatmentswereconducted at 450 °Cin a gas mixture of 25%N_2 + 75%H_2 under 4mbar.These optimal parameters are identified from the previous ASPN treatments reported [9]. This is because the ICR decreases with increasing the ASPN temperature but when the treatment temperature is above 450 °C, the formation of Cr precipitation will take place, thus leading to the serious degradation of corrosion resistance[11][12]. The treatment durationswere set for 7and 15h.In order to show the effect of Ag, normal ASPN treatment (i.e. ASP alloying with N) was also conducted with the same treatment conditions as for the ASPA(N&Ag) co-alloying treatments but only for 7 h.

After the plasma alloying treatments, scanning electron microscopy(SEM, Jeol 7000) and X-ray diffraction (XRD, Bruker D8 Advance) with Cu *Kα* radiation (λ=0.154nm)wereemployed to characterise the surface morphology and microstructure of the treated surfaces. Elemental depthprofiles weredetermined by glow discharge optical emission spectroscopy(GDOES).

The corrosion performance of both the treated and the untreated samples for comparison was evaluated by potentio-dynamic polarisation tests. A standard three-electrode system was used with a saturated calomel electrode (SCE) as the reference electrode. The electrolyte used was a sulphuric acid aqueous solution (0.5M H_2SO_4 + 2 ppm HF), and all the corrosion tests were conducted at room temperature.More details of the polarisation tests can be found in the previous publication [9].The surface electrical conductivity of all the samples was measured

using interfacial contact resistance (ICR) according to Wang's method [13] and the compaction pressureused for the ICR measurement was 1.4 MPa (140 N/cm^2).

3 Results

3.1 Surface morphology

The surface morphology of ASPA(N&Ag) and ASPN treated samples wereobserved by SEM. It can be seen from the low magnification images (Figure 1(a)(c)(e))that the surfaces are roughened after treatments with surface relief.Thisis a typical characteristic of the formation of S-phase mainly due to lattice expansion of grains with different orientations caused by the supersaturation of nitrogen[14].Under low magnification, the whole surface of 7h treated ASPN (Figure 1(a)) and 15h treated ASPA(N&Ag) (Figure 1(e)) is covered by fine white particles butit is interesting to find that only some areasof the 7h ASPA(N&Ag) treated surface are covered by the fine white particles, whichseem to correspond to the surface reliefor grains (denoted by white dash line in Figure 1 (c)).

The above varying contrast with grains observed on 7h ASPA(N&Ag) treated samples could be explained using the mechanism proposed by Corujeira Gallo & Dong [15].In their work, similar varying contrast with grains was observed under certain ASPN treatment conditions. This is mainly because the mass transfer of nitrogen in active screen plasma nitriding follows the following steps: deposition of iron nitride – their decomposition – inward diffusion of N. The diffusion of nitrogen in austenite grains and hence the decomposition of the deposited fine iron nitride particles on different grains is orientation dependent; the competetion between the deposition rate and the diffusion rate determine the resulted surafce morphology. If the deposition rate is much higher than the decomposition rate even for grains with most favourable (001) oriantationfor diffusion, more and more deposited particles will be piled up.Eventutally, a thick deposition layer covers the whole surafce, leading to the bright

contrast on the low magnification SEM pictures (Figures 1(a) and (c)); on the other hand, if the deposition rate is lower than the decomposition rate even for grains with least(111) favourable oriantation for diffusion, no large deposited particles would leave on the surface, thus leading to the dark constrast when observed under low magnification SEM. Only at a specific deposition rate, some grains are covered by such white deposited particles because they had unfavourable (111) oriantation for diffusion.

The deposition rate and the decompostiton rate are governed by many different aspects, such as the treatment temperature, duration and the chemical composition of the lid. For example, when treated under the same temperature (450°C) for the same time (7h), the deposition rate of iron nitride is faster in ASPN using a 316 SS screen than in ASPA(N&Ag) using a composites screen consisting of 316L SS doped with Agbecause of the presence of Ag in the lid and hence in the deposited layer. Hence, the whole surafce of the former was covered by the white particles whilst only some surafce areas of the latter showed similar white particles. The different surafce morphologies observed for 7h and 15h ASPA(N&Ag) treated surfacesmight be explainedby the longer time for the latter than for the former. This is because the diffusion coefficient of nitrogen in 316 SSwas found toreduce with the increase of low-temperature plasma treatment duration [16]and hence the amount of deposited particles would be expected to increase with prolonged treatment time.

The detailed surfaces morphology taken from the rectanglesshown in Figure 1 can be found in the high magnification SEM images (Figure 1 (b) (d) (f)). Many fine particles were observed on the surface of the 7h ASPN treated sample with the shape of polyhedron and the size of about 250nm in diameter (Figure 1 (b)). Particles can also be found on the surface of the 7h ASPA(N&Ag) treated surface; however, their size reduces to about 130nm in diameter. With the increase of the treatment duration to 15h, the size of the particles becomes un-even and the

average size increases to around 250nm on the surface of the 15h ASPA(N&Ag) treated sample.

The high magnification backscatter surface image of 15h ASPA(N&Ag) treated 316 SS (Figure 2 (a)) revealstwo different materials deposited on the surface, which can be deduced from the different contrasts. The EDS spectrums taken from the two areas with different contrasts (Figure 2 (b)), reveal that the bright area (Spectrum 1) is rich in Ag whilst the dark area (Spectrum 2) is rich in Fe. Considering the spatial resolution of EDS (≈1 μm) is larger than the thickness of the surface deposition layer (<0.5 μm), the EDS peaks of Fe, Cr, Ni and Si might come from the S-phase case underneath. Therefore, these bright particles might be metallic Ag particles as revealed from previous TEM observation [17].

3.2 Surface layer structure

3.2.1 XRD phase identification

The phase constituent of ASPA(N&Ag)and ASPN treated samples were analysed by XRD(Figure 3). The typical peaks of S-phase can be seen from the XRD charts of all the plasma treated samples. Comparedwith the peaks from the austenitic substrate, the peaks of S-phase areshifted to the lower angles because of the super-saturation of nitrogen in the austenite matrix.

Apart from S-phase, the peaks of silver and iron nitrides could also be identified from the ASPA(N&Ag) treated samples. The silver and iron were sputtered from the active screen lid and the iron reacted with nitrogen ions to form iron nitrides before deposited onto the sample surfaces. With the increase of the treatment duration, the surface deposition layer becomes thicker, thus contributing to the stronger peak intensity of silver and iron nitrides.However, no iron nitride peaks could be identified from theXRD chart for 7h ASPN treated 316 SS.

The above difference could be explained by the fact that the Ag particles in the deposition layer may have retarded the diffusion and hence decomposition of deposited iron nitrides. Hence, the peaks of silver and iron nitrides could be identified from the ASPA(N&Ag) treated samples; on the other hand, no peaks from the deposited iron nitride layer on ASPN 316 surface could be detected by XRDeither because the superficial layer of deposited particles is too thin to be detected by XRD or the observed surface particles would be the decomposition product of the deposited iron nitrides according to the deposition-decomposition-diffusion mechanism of active screen plasma processes.

In order to investigate the composition and structure of the as-deposited surface layer, ASPN and ASPA(N&Ag) treatments were also conducted on Si wafers in order to avoid the direct interaction and any mass transfer from the deposited layer to the stainless steel substrate. This is because the solid solubility of N in Si is extremely low and the diffusion of N in Si is difficult, if not impossible. Hence the composition and structure of the as-deposited layer could be retained after the treatment without the influence of the stainless steel substrate. From the XRD spectrums of 15h ASPN treated Si wafers (Figure 4), only peaks of iron nitrides can be detected from the ASPN treated Si surface, which supports the discussion in the last paragraph.For the ASPA(N&Ag) treated Si wafers, apart from the iron nitrides, the peaks of Ag could also be found. The XRD results reveal that the main phase constituents in the deposition layer of the ASPA(N&Ag) treatments are Ag and iron nitride, but in contrast, iron nitride is the only phase in that of the ASPN deposited surface layer.

3.2.2 GDOES depth profiles

The depth profiles of the elements across the plasma treated surface layer and the case beneath were generated using GDOES and the results are shown in Figure 5. The depth profiles of the major elements of 15h ASPA(N&Ag) treated sample are plotted inFigure 5(a). The profiles of Fe, N and Ag exhibit a peak in the near surface region, while the Cr profile

exhibits a trough in the same region. Beyond this surface region, no silver can be detected but the content of nitrogen decreases generally while other elements increases before reaching the substrate values.

The detailed depth distribution of Ag and N as a function of the ASPA(N&Ag) time is re-plotted in Figure 5 (b) and (c), respectively. The silver profiles of the ASPA(N&Ag) treated samples (Figure 5(b)) confirm the presence of silver in the ASPA(N&Ag) treated surfaces, and the depth of high-Ag region increases with the increase of treatment duration. The nitrogen profiles exhibit typical characteristic of S-phase reported in previous paper [9], and the nitrogen content, as well as the depth of high-nitrogen region, increase with the increase of treatment duration. When treated for the same duration, the ASPN treated sample exhibits higher and deeper nitrogen profile than that of the ASPA(N&Ag) treated sample.

3.2.3 Cross-sectional SEM images

TheSEM images of the cross-sectioned samples are shown in Figure 6. The low magnification images (Figure 6 (a)(b)(c)) show that featureless plasma modified surface caseswere formed after plasma surface treatments and the cases can be easily distinguished from the corroded substrate beneath. This implies that the plasmaco-alloyed surface cases are more resistant to the etchant used than the substrate. The thickness of these featureless cases correlates well with the nitrogen depth profiles shown in Figure 5 (c).Referring to the S-phase determined from the XRD results (Figure 3) and the very high nitrogen content, these cases can be identified as S-phase.

From the high magnification images taken from the un-etched cross-sections, a thin layer with different thicknesses can be observed on the very surface of the plasma treated samples. For the 7h ASPN treated sample (Figure 6(d)), the top surface layer is composed of many small particles, whicharepiled up loosely,and the layer thickness is not uniform. However, the top

surface layers formed on the surface of the ASPA(N&Ag) samples are dense, almost featureless and uniform in thickness. According to the literatures [18–21], the formation of these thin surface layerscould be explained according to the principles of active-screen plasma treatment: materials are sputtered from the active screen and then deposit onto the surface during the treatment.The thickness of the top surface layers matches well with the high silver region measured by GDOES (Figure 5(b)), indicating that the surface deposition layer is rich in silver.

The thickness of the surface deposition layer and the S-phase case underneath was measured from the cross-sectional SEM images and the results are presented in Figure 7. When treated at the same temperature for the same duration, both the surface deposition layer and the underneath S-phase case formed on the ASPA(N&Ag) treated sample are slightly thinner than that formed on the ASPN treated samples. This points towards different mechanisms involved in the ASPN and ASPA(N&Ag), which will be discussed in Section 4. For the ASPA(N&Ag) treated samples, the thickness of both the Ag-rich deposition layer and the S-phase case increase with the treatment duration.

3.3 Corrosion performance

The corrosion behaviour of ASPA(N&Ag) treated 316 SS was evaluated by potentio-dynamic polarisation tests. The polarisation curves of the ASPA(N&Ag) treated 316 SS samplesare plotted in Figure 8, together with the curves of untreated and 7hASPN treated sample for reference. The quantitative corrosion results in terms of corrosion potential and corrosion current density, obtainedfrom polarisation curves, aresummarised inTable I.

From the corrosion potential point of view, these two ASPA(N&Ag) treated samples exhibit,to some extent,more positive value than that of the untreated sample and 7h ASPN treated sample, which suggeststhe reducedcorrosion tendency, and the 15h ASPA(N&Ag)

treated sample showed the highest corrosion potential. It can also be seen from Table I that all the plasma treatments, namely ASPN and ASPA(N&Ag), can reduce the corrosion current density of 316 SS; furthermore when treated under the same temperature and duration, the ASPA(N&Ag) treated sample shows a much lower corrosion current densitythan the ASPN treated one. This finding proves that the addition of Ag has a positive effect in the improvement of the corrosion properties of 316 SS in terms of reduced corrosion current density and increased corrosion potential.

However, the passive current density of all the plasma treated 316 SS samples is higher than that of the untreated material. In general,the passive current density of all the samplesincreases in the order of untreated <ASPA(N&Ag)7h< ASPN 7h<ASPA(N&Ag)15h.

3.4 Surface electrical conductivity

The interfacial contact resistance (ICR) values of ASPA(N&Ag) treated samples arecompared in Figure 9with that of untreated and ASPN treated samples. The roughnessof all these measured samples is similar (about 0.12 ~ 0.15 μm). The ICR values of the ASPA(N&Ag) treated samples are around 20 mΩ cm^2, which isalmost one order of magnitude lower than that of the untreated one and two-thirdsof the ASPN treated sample. Clearly, the novel plasma co-alloying treatment developed from this research can effectively reduce the ICR of 316 austenitic stainless steel, and the plasma co-alloying with both N and Ag is more effective than ASP nitriding (i.e. alloying with N only).

4 Discussion

As has been reported above, the ASPA(N&Ag) treatments can significantly reduce the ICR value of 316 austenitic stainless steel (316 SS) from 157.8mΩ cm^2 to around 20mΩ cm^2; the ASPA(N&Ag) can also increase the corrosion potential and reduce the corrosion current

density of 316 SS. In addition, the ASPA(N&Ag) treated samples exhibit superior surface conductivity and corrosion behaviour to that of the ASPN treated sample. Therefore, it is of great importance to understand the mechanisms involved.

It is well-known that the surface conductivity and corrosion performance of a surface are closely related to itsstructure and composition. As compared in Figure 6, thesurface layerstructure of the ASPN treated and the ASPA(N&Ag) treated samples is similar, consisting of a top deposition layer and a underneath S-phase case. Therefore, it is reasonable to assume that the difference in surface properties should be related to the difference in the surface deposition layer formed by different treatments.

Naturally, this could be attributed to the essential difference between the ASPN treatment and ASPA(N&Ag) treatmentin the composition of the active-screen used. As described in Section 2, the whole active screen used for the ASPN is made of 316L SS, while for the ASPA(N&Ag) treatment, the lid of the active screen is composed of 5% Ag and 95% 316LSS. This should have led to the different compositionsand microstructure of the deposition layers.

From the XRD results shown in Figure 4, the main phase compositions of the ASPA(N&Ag)surface deposition layer are iron nitrides and silver particles. It is well known that metallic silver has excellent electrical conductivity. The silver particles embedin the deposition layer can act as electric current paths, thusfacilitating the flow of electric current and contributingto the reduced ICR value.

It is known that silver has a high standard electrode potential of 0.8V and is therefore regarded as a noble metal and possesses superior corrosion resistance[22]. In addition, the surface deposition layers on the ASPA(N&Ag) treated samplesare much denser than that of the ASPN treated samples (Figure 6), which could provide enhanced protection for the substrate against the acidic solution. Hence, the introduction of highly corrosion resistant

silver particles is expected to contribute to the increased corrosion potential and reduced corrosion current density (Table I) relative to the untreated and ASPN treated material. However, as discussed above, the surface deposition layer formed during the ASPA(N&Ag) consists of silver particles embedded in iron nitride. The difference in corrosion potential of these two phases would lead to galvanic corrosion. The relatively high passive current density of the ASPA(N&Ag) samples as compared to the untreated material (Figure 8) might be the consequence of the potential galvanic corrosion. Therefore, further research is required to tailor the phase constituentof the deposition layer to improve the corrosion behaviour of active scree plasma co-alloyed surfaces.

From the results of GDOES (Figure 5 (c)) and cross-sectional SEM (Figure 6), the ASPN treated surfaces exhibita higher nitrogen content and a thicker S-phase case than that of the ASPA(N&Ag) treated surfaces when treated under the same treatment duration. This could be explained by the introduction of Ag inASPA(N&Ag) treatment. It is well-documented that the iron nitrides formed in the deposited surface layer can act as nitrogen carrier which is essential for the formation of S-phase. During the ASPA(N&Ag) treatment, although the sputtered silver particles would not react with nitrogen, the deposition of silver will reduce the amount of nitrogen carriersdepositedon the surface being treated and the presence of Ag particles will retard the inward diffusion of nitrogen.These will reduce the supply of nitrogen, thus leadingto the lower nitrogen amount and thinner S-phase case of the ASPA(N&Ag) treated samples relative to the ASPN treated one.

5 Summary and Conclusions

A duplex surface layer structure, consisting of a silver-rich deposition layer and anunderneath high-nitrogen S-phase case, has been successfully generated by one-step active screen plasma

co-alloying technology with both interstitial element nitrogen and substitutional element silver. Experimental results demonstrate that metallic silver particlesare uniformly distributed in the iron nitride matrix within the surface deposition layer. The surface electrical conductivity tests have shown that the introduction of silver can significantly enhance the surface electrical conductivity of 316 austenitic stainless steel. Therefore, active screen plasma co-alloying with nitrogen and silvercould be a promising method to improve the surface properties of 316 SS for high-performancestainless steel bipolar plates in PEMFCs.

Acknowledgement

The financial support from European Commission (PIIF-GA-2012-327750) and EPSRC (EP/J018252/1) is gratefully acknowledged. One of the authors (KLin) wishes to express his appreciation to China Scholarship Council (CSC) and The University of Birmingham for their PhD studentships.

Reference

[1] T. Fukutsuka, T. Yamaguchi, S.-I. Miyano, Y. Matsuo, Y. Sugie, Z. Ogumi, Carbon-coated stainless steel as PEFC bipolar plate material, J. Power Sources. 174 (2007) 199–205. doi:10.1016/j.jpowsour.2007.08.096.

[2] D.. Davies, P.. Adcock, M. Turpin, S.. Rowen, Stainless steel as a bipolar plate material for solid polymer fuel cells, J. Power Sources. 86 (2000) 237–242. doi:10.1016/S0378-7753(99)00524-8.

[3] R. Tian, J. Sun, Performance of a high Cr and Ni austenitic stainless steel bipolar plates in proton exchange membrane fuel cell working environments, J. Power Sources. 194 (2009) 981–984. doi:10.1016/j.jpowsour.2009.06.027.

[4] S. Karimi, N. Fraser, B. Roberts, F.R. Foulkes, A review of metallic bipolar plates for proton exchange membrane fuel cells: Materials and fabrication methods, Adv. Mater. Sci. Eng. 2012 (2012). doi:10.1155/2012/828070.

[5] R. a. Antunes, M.C.L. Oliveira, G. Ett, V. Ett, Corrosion of metal bipolar plates for PEM fuel cells: A review, Int. J. Hydrogen Energy. 35 (2010) 3632–3647. doi:10.1016/j.ijhydene.2010.01.059.

[6] P. LIANG, H. XU, M. LIU, Electrochemical Performance Testing and Characterization of Silver-Plated and Graphite-Coated 316L Stainless Steel Bipolar Plates, Acta Physico-Chimica …. 26 (2010) 595–600. http://www.ingentaconnect.com/content/apcs/apcs/2010/00000026/00000003/art00012 (accessed September 9, 2014).

[7] Y. Fu, M. Hou, H. Xu, Z. Hou, P. Ming, Z. Shao, et al., Ag–polytetrafluoroethylene composite coating on stainless steel as bipolar plate of proton exchange membrane fuel cell, J. Power Sources. 182 (2008) 580–584. doi:10.1016/j.jpowsour.2008.04.051.

[8] K. Feng, Z. Li, X. Cai, P.K. Chu, Silver implanted 316L stainless steel as bipolar plates in polymer electrolyte membrane fuel cells, Mater. Chem. Phys. 126 (2011) 6–11. doi:10.1016/j.matchemphys.2010.11.029.

[9] K. Lin, X. Li, Y. Sun, X. Luo, H. Dong, Active screen plasma nitriding of 316 stainless steel for the application of bipolar plates in proton exchange membrane fuel cells, Int. J. Hydrogen Energy. 39 (2014) 21470–21479. doi:10.1016/j.ijhydene.2014.04.102.

[10] C.X. Li, J. Georges, X.Y. Li, Active screen plasma nitriding of austenitic stainless steel, Surf. Eng. 18 (2002) 453–457. doi:10.1179/026708402225006240.

[11] C.. Li, T. Bell, Corrosion properties of active screen plasma nitrided 316 austenitic stainless steel, Corros. Sci. 46 (2004) 1527–1547. doi:10.1016/j.corsci.2003.09.015.

[12] W. Liang, Surface modification of AISI 304 austenitic stainless steel by plasma nitriding, 211 (2003) 308–314. doi:10.1016/S0169-4332(03)00260-5.

[13] H. Wang, Stainless steel as bipolar plate material for polymer electrolyte membrane fuel cells, J. Power Sources. 115 (2003) 243–251. doi:10.1016/S0378-7753(03)00023-5.

[14] H. Dong, S-phase surface engineering of Fe-Cr, Co-Cr and Ni-Cr alloys, Int. Mater. Rev. 55 (2010) 65–98. doi:10.1179/095066009X12572530170589.

[15] S. Corujeira Gallo, H. Dong, New insights into the mechanism of low-temperature active-screen plasma nitriding of austenitic stainless steel, Scr. Mater. 67 (2012) 89–91. doi:10.1016/j.scriptamat.2012.03.028.

[16] T. Moskalioviene, A. Galdikas, Stress induced and concentration dependent diffusion of nitrogen in plasma nitrided austenitic stainless steel, Vacuum. 86 (2012) 1552–1557. doi:10.1016/j.vacuum.2012.03.026.

[17] Y. Dong, X. Li, R. Sammons, H. Dong, The generation of wear-resistant antimicrobial stainless steel surfaces by active screen plasma alloying with N and nanocrystalline Ag., J. Biomed. Mater. Res. B. Appl. Biomater. 93 (2010) 185–93. doi:10.1002/jbm.b.31573.

[18] C.X. Li, T. Bell, H. Dong, A Study of Active Screen Plasma Nitriding, Surf. Eng. 18 (2002) 174–181. doi:10.1179/026708401225005250.

[19] C. Zhao, C.X. Li, H. Dong, T. Bell, Study on the active screen plasma nitriding and its nitriding mechanism, Surf. Coatings Technol. 201 (2006) 2320–2325. doi:10.1016/j.surfcoat.2006.03.045.

[20] S. Corujeira Gallo, H. Dong, On the fundamental mechanisms of active screen plasma nitriding, Vacuum. 84 (2009) 321–325. doi:10.1016/j.vacuum.2009.07.002.

[21] A. Nishimoto, T. Matsukawa, H. Nii, Effect of Screen Open Area on Active Screen Plasma Nitriding of Austenitic Stainless Steel, ISIJ Int. 54 (2014) 916–919. doi:10.2355/isijinternational.54.916.

[22] J. Song, L. Wang, A. Zibart, C. Koch, Corrosion Protection of Electrically Conductive Surfaces, Metals (Basel). 2 (2012) 450–477. doi:10.3390/met2040450.

Table IThe results of potentio-dynamic polarization tests

Sample	Corrosion potential (mV vs SCE)	Corrosion current density (mA/cm^2)
UNT	-460	0.114
ASPN 7h	-443	0.088
ASPA(N&Ag) 7h	-427	0.021
ASPA(N&Ag) 15h	-417	0.097

Figure 1
SEM morphology of treated surfaces: Low magnification (a) ASPN 7h (c) ASPA(N&Ag) 7h (e) ASPA(N&Ag) 15h; High magnification (b) ASPN 7h (d) ASPA(N&Ag) 7h (f) ASPA(N&Ag) 15h

Figure 2
Analysis of 15h ASPA(N+Ag) treated 316 SS under high magnification(a) Surface backscatter image (b) EDS spectrums of two points

Figure 3
XRD spectrums of different samples

Figure 4
XRD patterns of ASPA (N&Ag) and ASPN treated Si wafer after 450°C/15h treatment

Figure 5
Depth profiles of (a) main elements in 15h ASPA(N&Ag) treated surfaces, (b) nitrogen and (c) silver as a function of treatment time

Figure 6
Cross-sectional SEM image of different samples: low magnification (a) ASPN 7h (b) ASPA(N&Ag) 7h (c) ASPA(N&Ag) 15h; high magnification (d) ASPN 7h (e) ASPA(N&Ag) 7h (f) ASPA(N&Ag) 15h

Figure 7
The thickness of S-phase layer and deposition layer on different treated samples

Figure 8
The potentio-dynamic polarization curves of different samples

Figure 9
The ICR results of different 316 SS samples

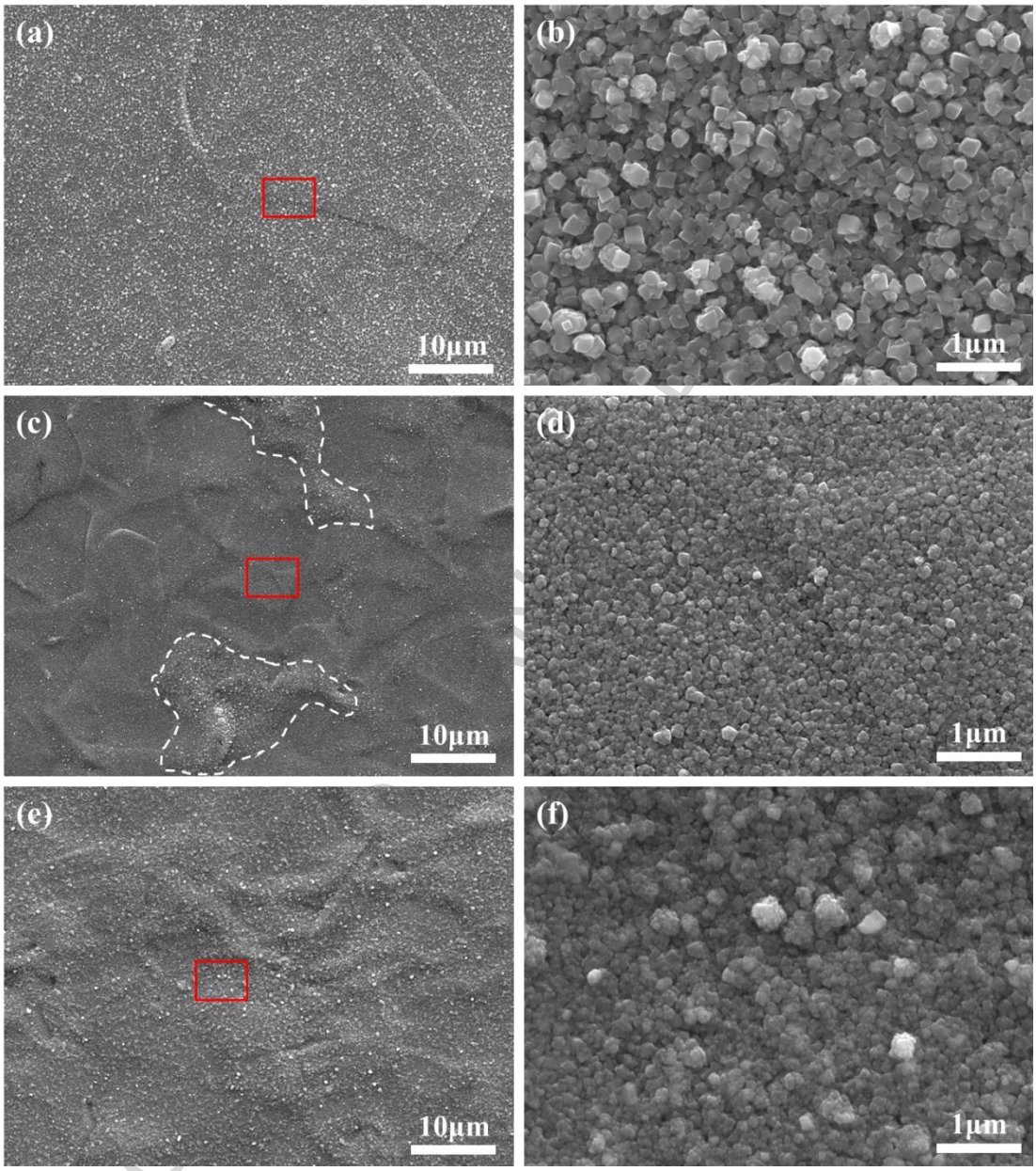

Figure 1

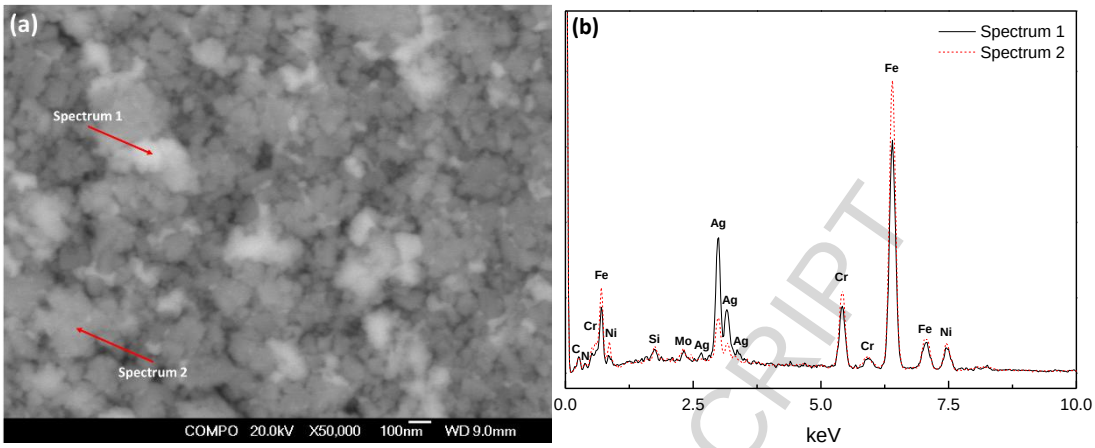

Figure 2

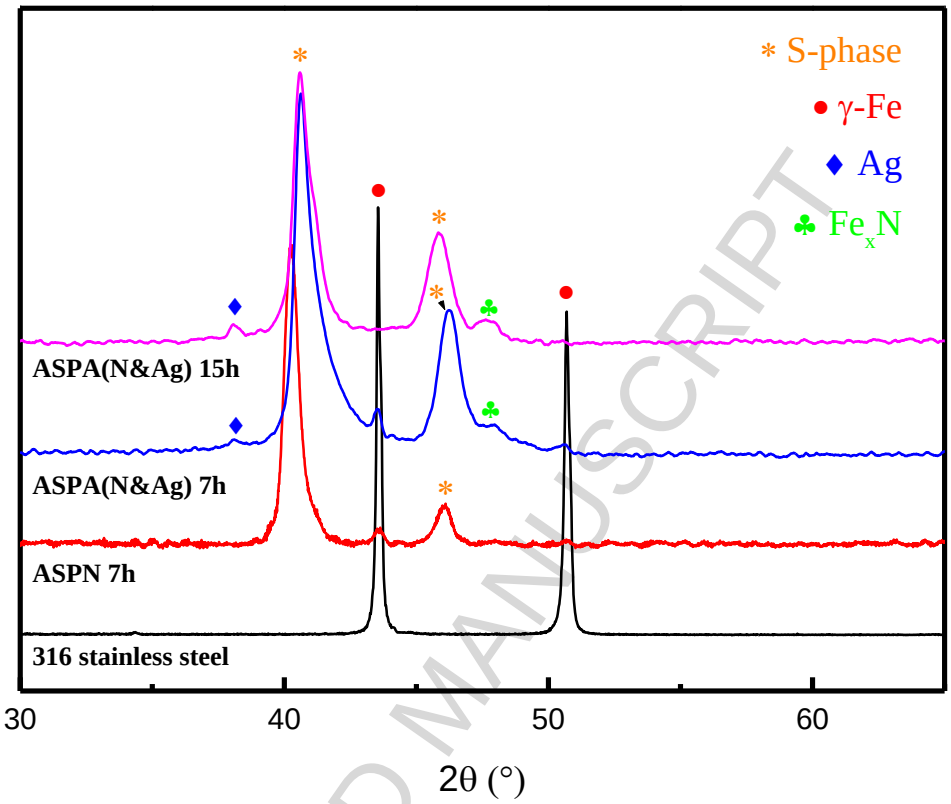

Figure 3

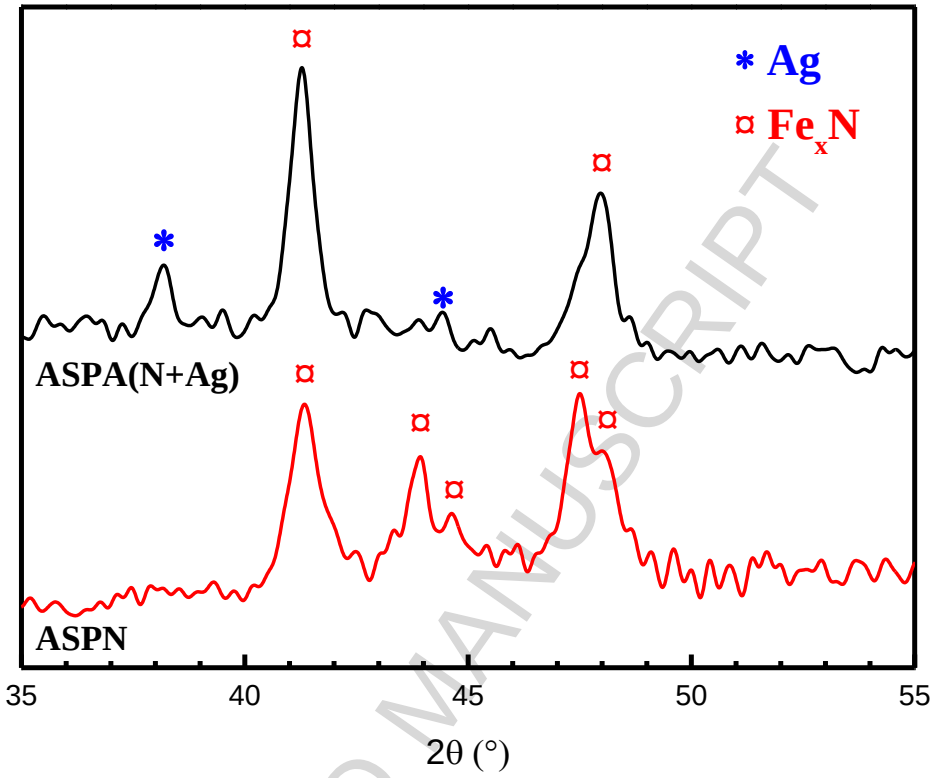

Figure 4

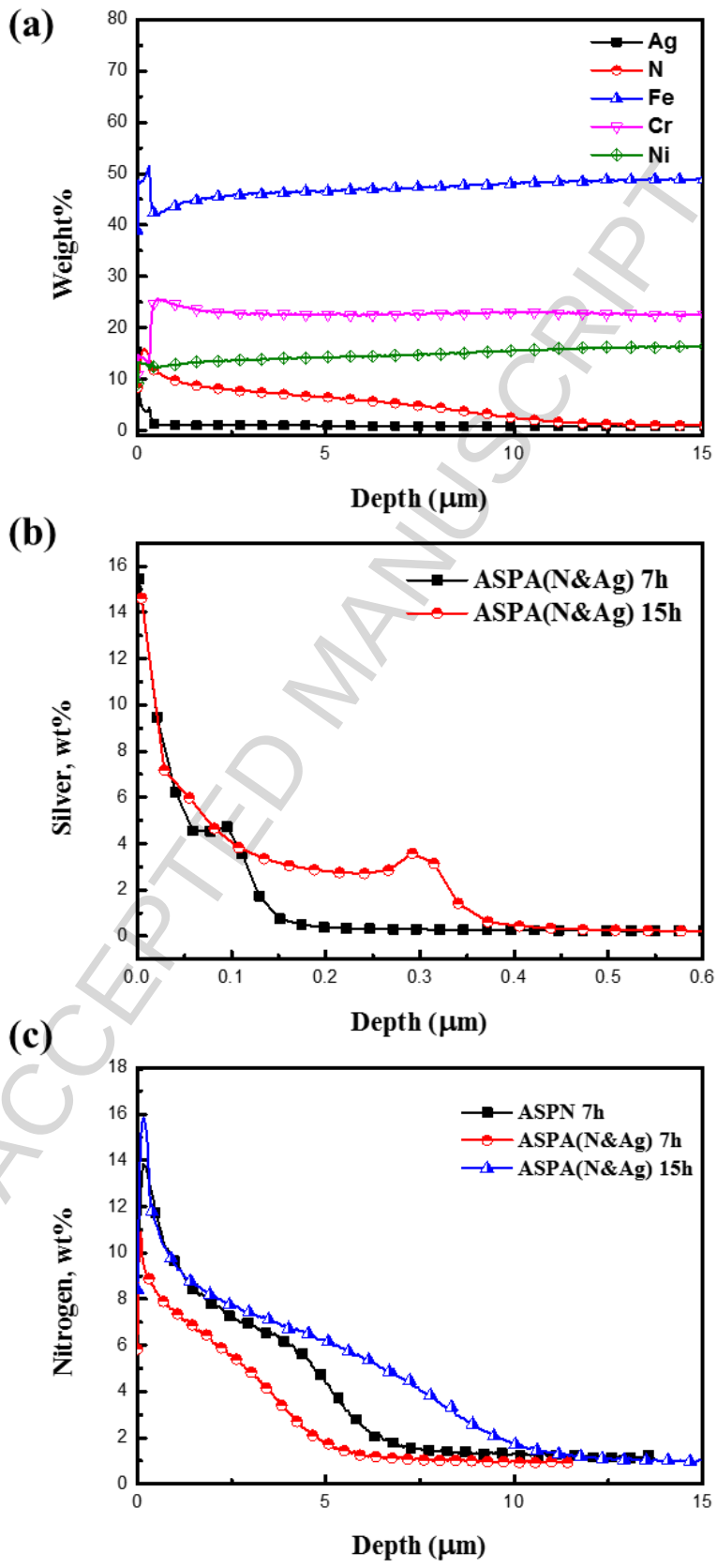

Figure 5

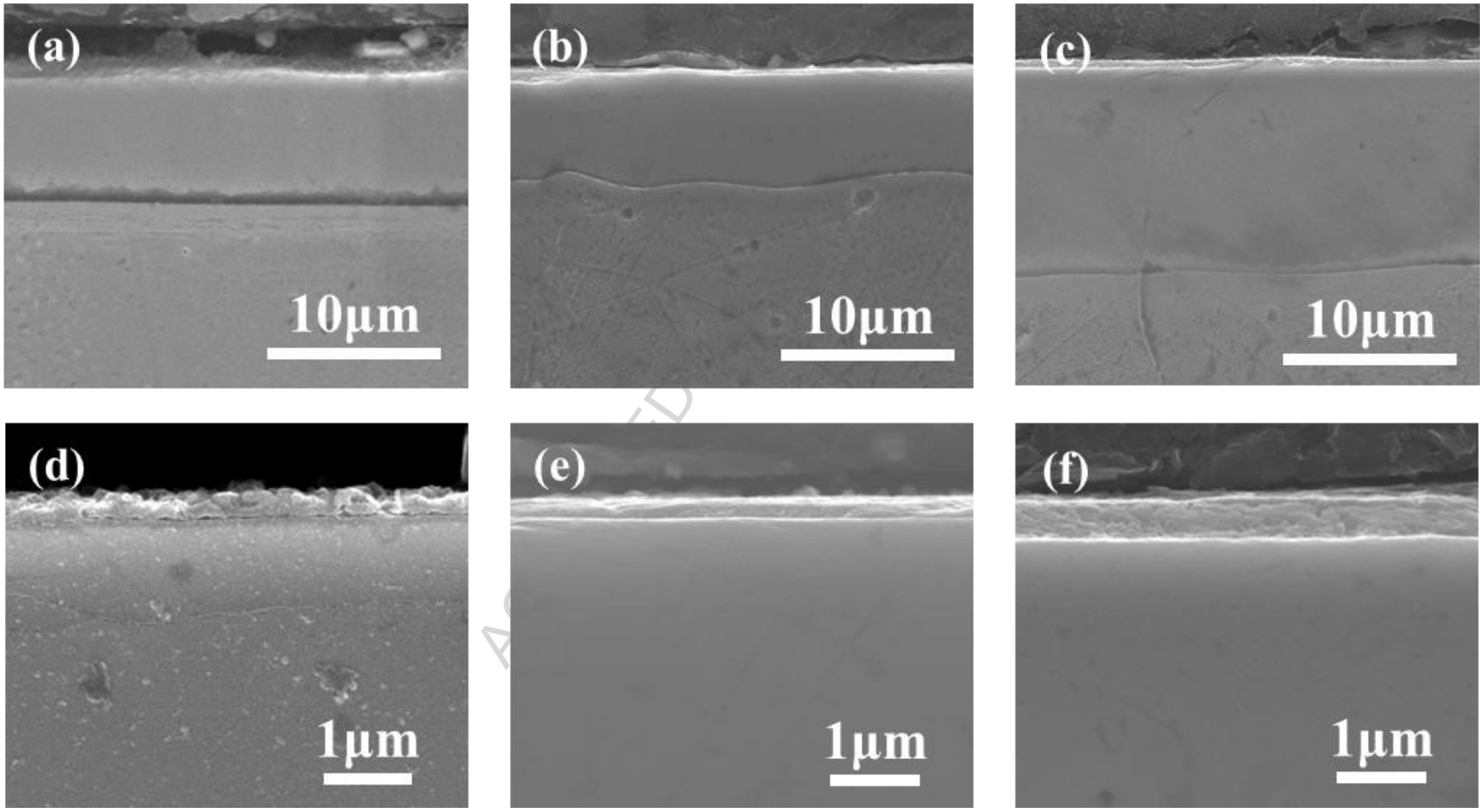

Figure 6

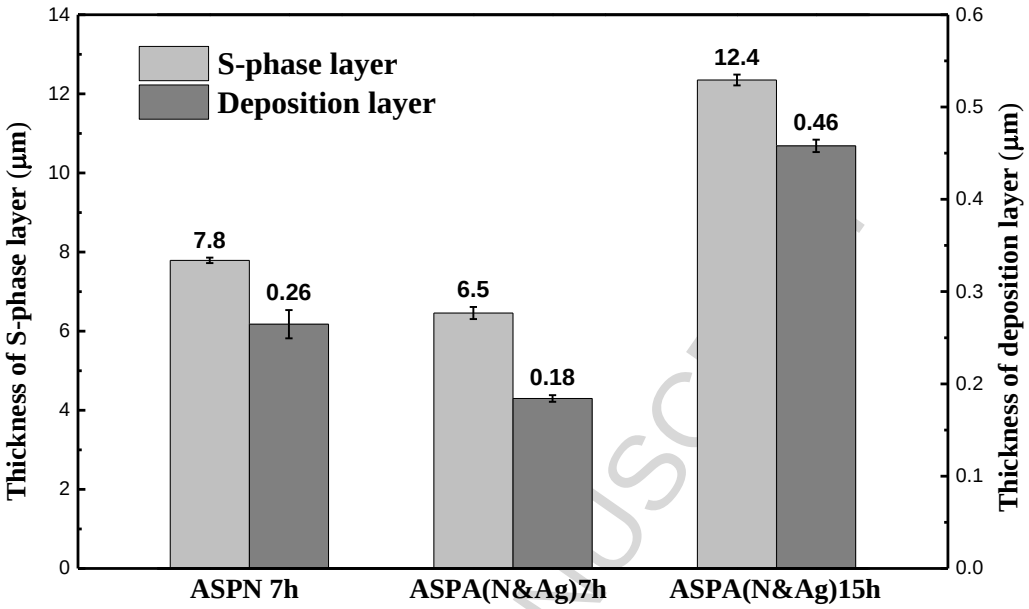

Figure 7

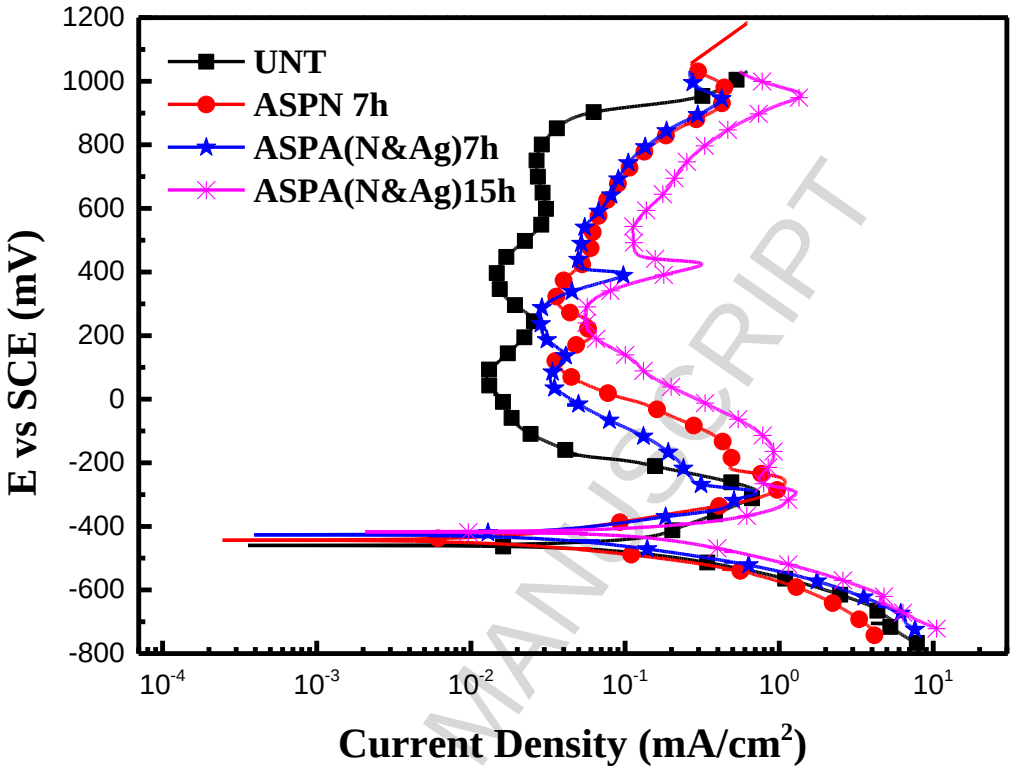

Figure 8

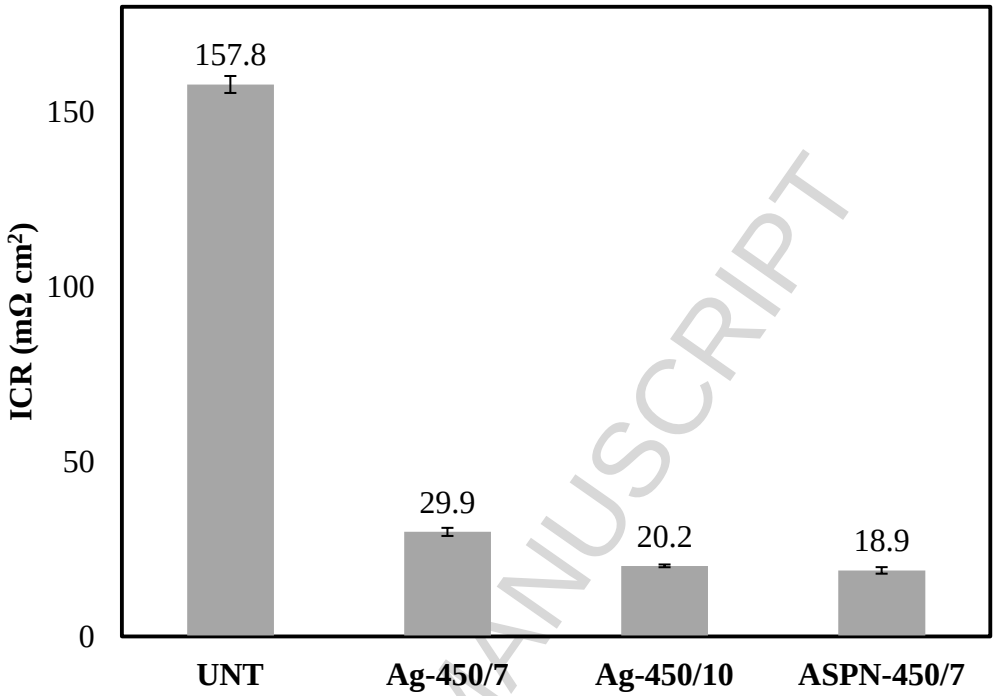

Figure 9

Highlights

- Radically reduced interfacial contact resistance of 316 by surface N/Ag co-alloying
- A duplex surface layer structure produced by one-step plasma surface treatment